Nuclear fusion induced by X-rays in a crystal

V.B. Belyaev[1] * , M.B. Miller[2], J. Otto[3], S.A. Rakityansky[3] †

[1] Joint Institute for Nuclear Research, Dubna, Russia

[2] Institute for Physical and Technical Problems, Dubna, Russia

[3] Dept. of Physics, University of Pretoria, Pretoria, South Africa

March 8, 2016

Abstract

The nuclei that constitute a crystalline lattice, oscillate relative to each other with a very low energy that is not sufficient to penetrate through the Coulomb barriers separating them. An additional energy, which is needed to tunnel through the barrier and fuse, can be supplied by external electromagnetic waves (X-rays or the synchrotron radiation). Exposing to the X-rays the solid compound LiD (lithium-deuteride) for the duration of 111 hours, we have detected 88 events of the nuclear fusion $d + {}^6\mathrm{Li} \to {}^8\mathrm{Be}^*$. Our theoretical estimate agrees with what we observed. One of possible applications of the phenomenon we found, could be the measurements of the rates of various nuclear reactions (not necessarily fusion) at extremely low energies inaccessible in accelerator experiments.

1 Introduction

Fusion of two atomic nuclei is possible if they approach each other to a short distance ($\sim 10^{-13}$ cm). To come that close, they need to go through a Coulomb barrier of the height of few MeV. The penetration probability for such a barrier at room temperature (energy of relative motion ~ 10 meV) is practically zero ($\sim 10^{-2600}$ [1]), but this probability rapidly grows when the kinetic energy of the nuclei increases. For example, for the dd system at the energy

*Passed away in March 2015

†e-mail: rakitsa@up.ac.za

of 30 keV the penetration probability becomes $\sim 10^{-3}$ [1]. Therefore, the obvious way to fuse the nuclei is to raise the temperature of their mixture. In this way the so called thermo-nuclear reactions happen in the stellar bodies, in nuclear weapons, and in the TOKAMAK [2].

Alternatively, the nuclei (which we want to fuse) can be put in a bound system such as a molecule, where they sit next to the barrier relatively long. In such a case, even at zero relative energy, the nuclei are separated by a thinner barrier. For example, the two deuterons sitting at rest near each other at a distance of 1Å, have to overcome the same barrier as two free moving deuterons with relative energy of $14\,\text{eV}$ (which is equivalent to the temperature of $\sim 1.6 \times 10^5\,^\circ\text{K}$).

This, however, does not help much. For a deuterium molecule D_2 in its ground state the penetration probability is still too low, namely, $\sim 10^{-82}$ [1] and the fusion rate is $\sim 10^{-62}\,\text{s}^{-1}$ [3]. These numbers can be significantly increased if we make the size of the molecule smaller. This can be achieved if one electron in the molecule is replaced with the muon, which is approximately 200 times heavier. As a result, the nuclei find themselves at a distance that is 200 times smaller [4,5]. For the deuterons, the thickness of the barrier becomes the same as at the collision energy almost equal to 3 keV (this corresponds to the temperature of $\sim 30 \times 10^6\,^\circ\text{K}$).

This is already a significant gain. The penetration probability for the muonic molecule $dd\mu$ is $\sim 10^{-6}$ [1,6]. With such a probability, one muon can help to fuse, i.e. can catalyze the fusion of many nuclear pairs before it decays (muon lifetime is $\sim 2 \times 10^{-6}\,\text{s}$). The muon-catalyzed fusion has been observed and well studied both experimentally and theoretically (see, for example, Refs. [6,7]), but turned out to be inefficient as a new source for the energy production.

In the present paper, we suggest and experimentally explore yet another possible approach to fusion of light nuclei. The idea is to make a crystal out of the atoms whose nuclei we want to fuse. In this crystal, the nuclei sit next to each other at an atomic distance and oscillate around the equilibrium positions. A crystal is just a huge molecule and of course the probability of spontaneous fusion of neighbouring nuclei is negligible, the same as in the ordinary molecules. An experiment aimed to observe the spontaneous fusion in the lithium deuteride crystal put an upper bound on the fusion rate per nuclear pair as $\sim 10^{-48}\,\text{s}^{-1}$ [8].

However, we can try to shake the crystalline lattice by an external force (electromagnetic wave, for example). The nuclei swayed around their equilibrium positions, acquire kinetic energy relative to each other. As a result, the original Boltzmann distribution of the nuclei over the oscillation levels is changing and the higher levels are populated. From these higher energy levels the nuclei can tunnel through the Coulomb barrier and fuse. This is what we

observed when irradiated the LiD crystal with the X-rays. The rate of such a fusion turned out to be very low (one event every half an hour), but still easily measurable.

2 Nuclear subsystem

2.1 Fusion channels

The nuclei we want to fuse, are the isotopes of hydrogen and lithium, namely, $^2\mathrm{H}$ and $^6\mathrm{Li}$. Their compound nucleus, $^8\mathrm{Be}$, has no stable states. The threshold energies for its spontaneous disintegration in various pairs of fragments are shown in Fig. 1 (the data are taken from Ref. [9]). As is seen, the d-$^6\mathrm{Li}$ threshold lies $22.2808\,\mathrm{MeV}$ above the ground state (which is

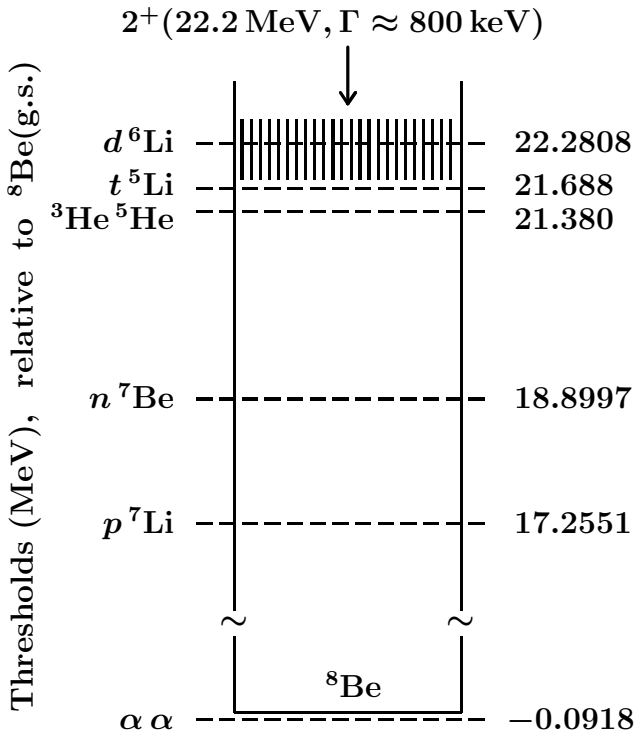

Figure 1: Threshold energies (in MeV) for various two-cluster arrangements of the nucleons constituting $^8\mathrm{Be}$ nucleus. The energies are shown relative to the ground state of $^8\mathrm{Be}$. A wide meta-stable state (2^+) of this nucleus is shown around the $d\,^6\mathrm{Li}$ threshold.

also unstable). And this is above the thresholds for all the other two-body channels, namely,

$t\,^5\mathrm{Li}$, $^3\mathrm{He}\,^5\mathrm{He}$, $n\,^7\mathrm{Be}$, $p\,^7\mathrm{Li}$, and $\alpha\,\alpha$.

When sitting at the nodes of a crystalline lattice, the nuclei oscillate around their equilibrium positions, but the oscillation energy is negligible on the nuclear scale. They therefore can be considered as being at rest relative to each other. In other words, the nuclear pair $d\,^6\mathrm{Li}$ in a crystal is practically at the threshold energy.

If d and $^6\mathrm{Li}$ in the crystal, overcome huge Coulomb barrier and fuse, then there is no way back for them. Indeed, for the resulting excited (resonant) state $^8\mathrm{Be}^*$ to decay back into the channel $d + {}^6\mathrm{Li}$, the deuteron and lithium nuclei must overcome the same huge Coulomb barrier, while they have practically zero relative kinetic energy. It is much more easier to decay into one of the channels whose thresholds are below and where the kinetic energy is above the Coulomb barrier. For example, in the channel $\alpha + \alpha$ (which lies $0.0918\,\mathrm{MeV}$ below the ground state of the compound nucleus) the relative kinetic energy is greater than in the $d\,^6\mathrm{Li}$ channel by the amount of $22.2808\,\mathrm{MeV} + 0.0918\,\mathrm{MeV} = 22.3726\,\mathrm{MeV}$, i.e. is always well above the barrier.

If we restrict our model consideration to only the two-body channels, then our 8-body problem involves six-channels, namely,

$$d + {}^6\mathrm{Li} \;\rightarrow\; \begin{cases} d + {}^6\mathrm{Li} \\ t + {}^5\mathrm{Li} + 0.5928\,\mathrm{MeV} \\ {}^3\mathrm{He} + {}^5\mathrm{He} + 0.9008\,\mathrm{MeV} \\ n + {}^7\mathrm{Be} + 3.3811\,\mathrm{MeV} \\ p + {}^7\mathrm{Li} + 5.0257\,\mathrm{MeV} \\ \alpha + \alpha + 22.3726\,\mathrm{MeV} \end{cases} \tag{1}$$

and all of these channels are open. In other words, if d and $^6\mathrm{Li}$ fuse, the final outcome would be one of the pairs on the right hand side of Eq. (1) with the energy release shown for each channel.

Around the $(d + {}^6\mathrm{Li})$-threshold, the compound nucleus $^8\mathrm{Be}$ has several very wide and overlapping meta-stabele states (resonances). The one that is located most closely to the threshold, has the quantum numbers: (total spin and parity) $J^\pi = 2^+$, (isospin) $T = 0$,

$E = 22.2\,\mathrm{MeV}$, and $\Gamma \approx 0.80\,\mathrm{MeV}$ [9]. This wide state is shown in Fig. 1 as a strip of verdical bars.

Recent analysis of experimental data, based on the R-matrix parametrization [10], showed that at the near-threshold energies the inelastic collision of d and $^6\mathrm{Li}$ mainly leads to formation of that resonance $^8\mathrm{Be}^*(2^+, 0, 22.2\,\mathrm{MeV})$. The authors of Ref. [10] also showed that this resonance predominantly decays into the $\alpha\alpha$-channel. They found that the partial width for such a decay is $\Gamma_\alpha = 0.77\,\mathrm{MeV}$, which gives $\Gamma_\alpha/\Gamma \approx 0.96$. In other words, after its formation, this resonance decays in the $\alpha\alpha$-channel with the probability of 96%.

Ignoring the remaining 4%, we can assume that, if the fusion of our d and $^6\mathrm{Li}$ happens, almost the only outcome is the $\alpha\alpha$ pair,

$$d + {}^6\mathrm{Li} \;\longrightarrow\; \alpha + \alpha \;. \tag{2}$$

The resulting α-particles equally share the energy and momentum. Therefore the fusion event could be identified by detecting at least one of the two α-particles moving in the opposite directions with the energies of $11.1863\,\mathrm{MeV}$.

2.2 Fusion rate

Nuclear reactions at extremely low energies ($E \sim 10\,\mathrm{keV}$) are significantly suppressed by the repelling Coulomb forces. The probability $T(E)$ that the colliding nuclei tunnel through the Coulomb barrier is equal to the ratio $|\psi_E(0)|^2/|\psi_E(R_c)|^2$, where $\psi_E(r)$ is the wave function of their relative motion at the distance r, and R_c is the classical turning point. It can be shown (see Eq. (134.10) of Ref. [11]) that for a pure Coulomb potential, the ratio of $|\psi_E(0)|^2$ to absolute square of the plane wave is given by

$$T(E) = \frac{2\pi\eta}{\exp(2\pi\eta) - 1} \quad \underset{E\to 0}{\longrightarrow} \quad 2\pi\eta\exp(-2\pi\eta)\;, \tag{3}$$

where

$$\eta = \frac{Z_1 Z_2 e^2}{\hbar}\sqrt{\frac{\mu}{2E}} \tag{4}$$

is the Sommerfeld parameter that involves the nuclear charges, Z_1 and Z_2, and the reduced mass μ of the nuclear pair. For the purpose of estimating, we can assume that for distances $r > R_c$ the relative motion of the nuclei in the crystalline cell is described by a plane wave, and thus Eq. (3) gives us the penetration probability for the Coulomb barrier.

In our problem, the nuclei are confined to finite volumes of space in the crystal. Within its cell, a nucleus moves to and fro, periodically colliding with the barriers. Each of these collisions is an attempt to tunnel through. If the size of the cell is D and velocity of the nucleus is v, then the attempts are repeated with the period $2D/v$, i.e. with the frequency $\nu = v/2D$.

Therefore, the number of transitions through the barrier per second (i.e. the transition rate) is $T\nu$. As we mentioned in Sec. 2.1, if the deuteron (or $^6\mathrm{Li}$) manages to pass to the other side of the barrier, there is no way back (for that, it needs to tunnel once more through the same barrier, while the penetration probability is very small). This means that if the penetration takes place, the nuclear system ends up in one of the inelastic channels given by Eq. (1). Among these channels, the reaction (2) has the highest probability, $\gamma_\alpha = 0.96$. Therefore, if a deuteron in the crystal oscillates with the energy E, the reaction (2) happens with the rate

$$W_d(E) = \frac{T(E)\gamma_\alpha}{2D}\sqrt{\frac{2E}{\mu_d}}\ , \tag{5}$$

where μ_d is the mass of deuteron. Apparently, the same is valid for the tunneling of a lithium nucleus, and the corresponding reaction rate $W_{\mathrm{Li}}(E)$ can be obtained in the same way.

3 Crystal

3.1 Structure

Lithium hydride is an ionic crystal with simple cubic structure. In each pair of Li and D atoms, one electron is transferred from the lithium to the deuterium. As a result, the crystal consists of positive ions of lithium and negative ions of deuterium. The extra electron is loosely bound to the deuterium, which makes the radius of the ion D^- approximately twice as much as the radius of Li^+ (see, for example, Ref. [12]). Schematically, the structure of lithium deuteride crystal is depicted in Figures 2 and 3.

3.2 Inter-nuclear potential

If we consider just bare nuclei sitting at the nodes of the lattice, they repel each other with the Coulomb forces and at short distances attract each other with the strong forces. The surrounding electrons make the configuration stable and partly screen the Coulomb repulsion. For a deuteron nucleus, the neighbouring $^6\mathrm{Li}$ nuclei create the potential profile schematically shown in Fig. 4. There are three orthogonal axes along which the deuteron moves in such

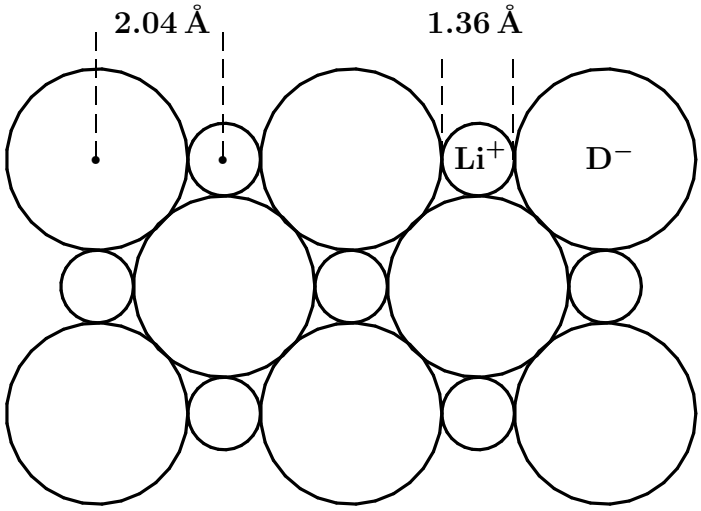

Figure 2: Schematic picture of one layer of LiD crystal. The indicated distances are taken from Ref. [12].

a potential. In order to fuse with ^{6}Li, the deuteron have to tunnel through one of the six potential barriers surrounding it.

The height $V_{\max}$ of the barrier can be estimated as the Coulomb repulsion energy of the charges $Z_1 = 1$ and $Z_2 = 3$ at the distance $r_1 + r_2$, where $r_1 = 2.1424\,\mathrm{fm}$ [13] and $r_2 = 2.5432\,\mathrm{fm}$ [14] are the nuclear radii of the deuteron and ^{6}Li, respectively. This gives

$$V_{\max} \approx \frac{Z_1 Z_2 e^2}{r_1 + r_2} \approx 0.922\,\mathrm{MeV}\ .$$

Apparently, the central minimum of the potential shown in Fig. 4, is not the same as the zero potential energy for an isolated $d\,^6\mathrm{Li}$ pair. Indeed, the deuteron is pushed away from both sides. This effectively lifts the deuteron up against the barrier.

If $R_0 = 2.04\,\mathrm{Å}$ is the distance between the nuclei d and ^{6}Li in the crystal [12], and x is the shift of the deuteron from its equilibrium position, then the Coulomb forces acting on it from the neighbouring lithium nuclei, generate the potential energy:

$$V(x) = \frac{Z_1 Z_2 e^2}{R_0 - x} + \frac{Z_1 Z_2 e^2}{R_0 + x}\ . \tag{6}$$

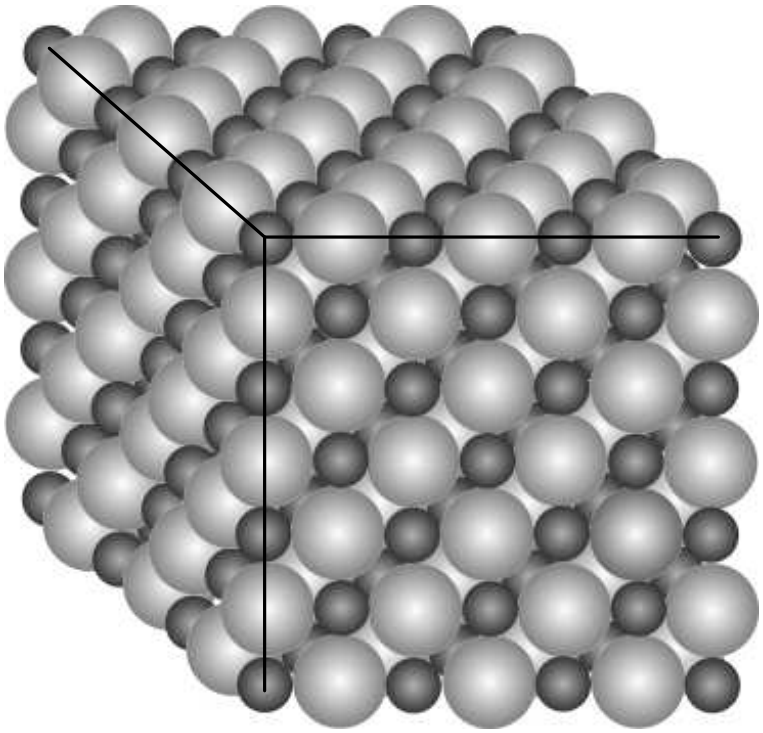

Figure 3: Schematic 3-dimensional picture of LiD crystal.

At the equilibrium point ($x = 0$) the potential is

$$V_{\min} = \frac{2Z_1 Z_2 e^2}{R_0} \approx 42.35\,\mathrm{eV}\ . \tag{7}$$

This is how much the deuteron in the crystal is lifted up against the free-space Coulomb barrier. Actually, the deuteron energy is even a bit higher. This additional energy, however, is associated with the thermal oscillations and therefore is small, namely, of the order of $\sim k_B T$, i.e. $\sim 25\,\mathrm{meV}$ at room temperature.

The deuteron sitting in the central well of the potential shown in Fig. 4, oscillates around its equilibrium point. In order to estimate the fusion rate, we need to know the energy levels (spectrum) of its oscillations, as well as the distribution of the statistical ensemble of the deuterons over these levels. For the estimation purpose, this problem can be simplified if we approximate the central well by another potential for which both the spectrum and wave functions are known analytically.

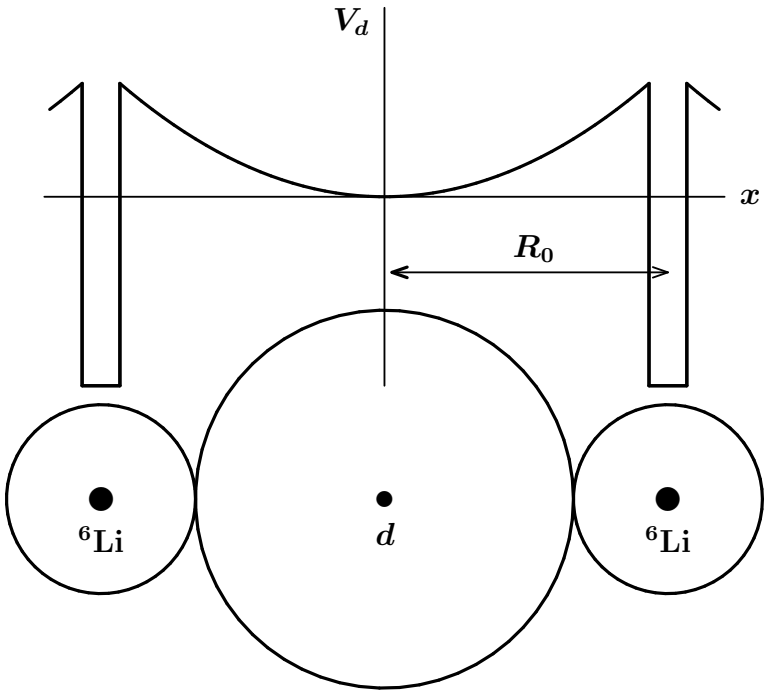

Figure 4: Schematic picture of the potential energy of a deuteron nucleus in the Coulomb and nuclear fields of the two neighbouring lithium atoms. The potential energy is considered along the line connecting the centers of these atoms.

Looking at Fig. 4, one might guess that the best approximation would be a parabola, i.e. a harmonic oscillator potential. This however is wrong because the curve shown in that figure is schematic. Actually, if we accurately plot the function (6) on the interval $-R_0 + (r_1 + r_2) \leqslant x \leqslant R_0 - (r_1 + r_2)$, it is practically flat everywhere except for the left and right ends of this interval, where it quickly raises to $V_{\max}$. The reason is that R_0 is too large as compared to the range of distances where the Coulomb potential is comparable with $V_{\max}$. Actual potential-well looks as is shown in Fig. 5, where we removed the central part, which is long and almost flat.

Of course, in addition to the Coulomb fields generated by the nuclei, there are also electric fields due to the electron shells of the ions. However, these fields are weak as compared to the height $V_{\max} \approx 0.922\,\mathrm{MeV}$ of the Coulomb barriers. Indeed, the binding energy of an electron to the nucleus (and therefore of the nucleus to the shell) in a hydrogen atom is $\sim 13\,\mathrm{eV}$, which is five orders of magnitude smaller than the height of the barrier. The reason of relative weakness of the electron field in the crystal is that, in contrast to the nuclei, the electrons

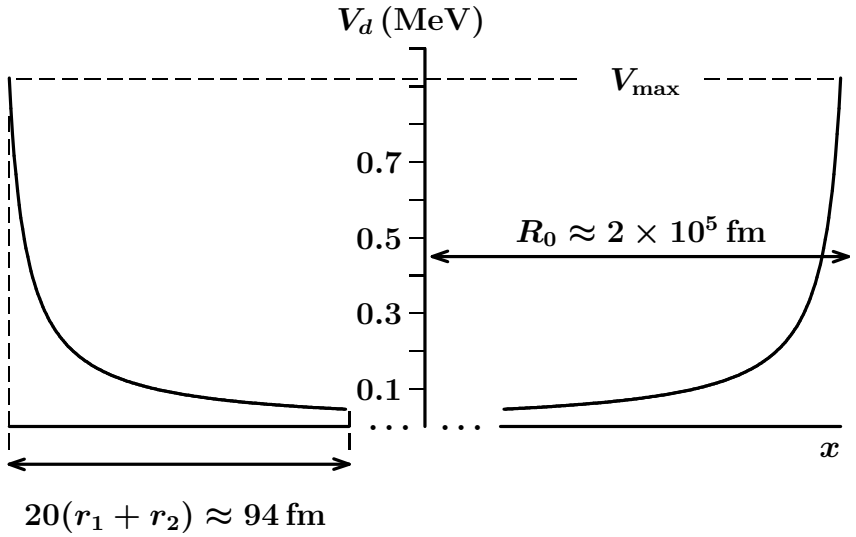

Figure 5: The potential energy of a deuteron nucleus in the Coulomb fields of the two neighbouring lithium nuclei. The potential energy is considered along the line connecting the centers of these nuclei. There are shown only the leftmost and rightmost segments of this line. The central part (which is three orders of magnitude longer) is cut out because it is practically flat.

act not as point-like charges but as a space charge of the electron cloud distributed within a volume of few Angstrom size.

For the purpose of estimating, we can assume that the electron cloud is a uniformly charged sphere. For a charge $Z_1 e$, the interaction potential with the charge Ze uniformly distributed within a sphere of radius R, is (see Eq. (2-104) of Ref. [15])

$$V_{\rm sphere}(r) = \frac{Z_1 Z e^2}{2R}\left(3 - \frac{r^2}{R^2}\right) \ , \qquad r \leqslant R \ , \tag{8}$$

where r is the distance of charge $Z_1 e$ from the centre of the sphere. If we assume (for the sake of estimating) that the electron shell of the ion $\rm D^-$ is a uniformly charged sphere ($Z = 2$) of the radius $R_{\rm D} = 1.36\,\text{Å}$ ($R_{\rm D} = 2R_{\rm Li}$: see Fig. 2), then the strongest attraction (at $r = 0$) for the deuteron from its own electron shell is $3e^2/R_{\rm D} \approx 32\,{\rm eV}$. In other words, the bottom of the potential shown in Fig. 5, is not exactly flat. At its centre, it has an additional shallow "dent" (potential well) of the depth $\sim 30\,{\rm eV}$, which is spherically spread to a distance of $\sim 1.36\,\text{Å}$.

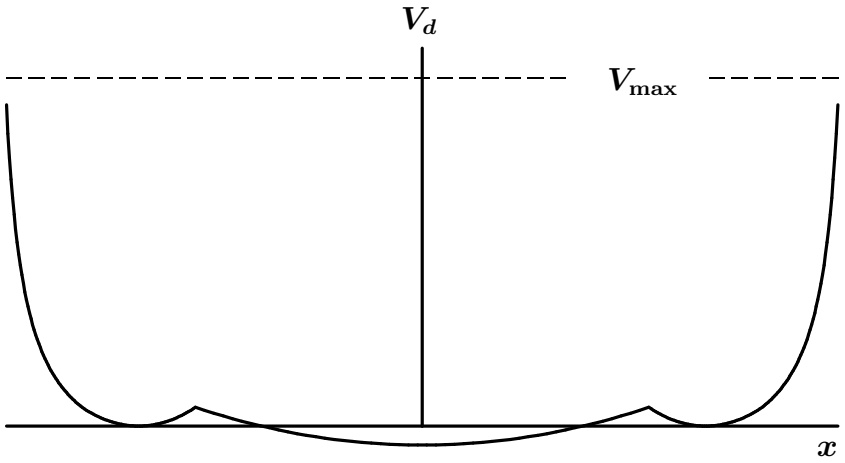

Figure 6: The potential energy of a deuteron nucleus in the Coulomb fields of the two neighbouring lithium nuclei modified by the attractive fields of the electronic shells. This is a schematic picture: the scale is distorted for the sake of showing the effect of the electron clouds. As a result of the distortion, this effect is exaggerated here.

Similarly, within the electron cloud of the Li^+ ion, there is another "dent" on the potential curve of the depth $\sim 60\,\mathrm{eV}$ (because the radius of this cloud is half of the deuterium radius). Therefore the potential energy of the deuteron nucleus in the crystal (along the line connecting two neighbouring lithium nuclei) looks like is schematically shown in Fig. 6.

It should be noted that despite its depth, the bottom of the lithium "dent" is a bit higher relative to the deuterium one because it is superimposed on the center of the Coulomb repulsion. It is clear that such a superposition slightly reduces both the height and the thickness of the Coulomb barrier. Of course the curve shown in Fig. 6, is an exaggeration. Actual depths of the "dents" are five orders of magnitude smaller than the height $V_{\max}$ of the barrier. This means that, if plotted correctly, actual curve looks practically as a square-well potential of the depth $V_{\max}$ and width $2R_0$. It should be emphasized that we can only ignore the electron "dents" when consider the motion of the deuteron along any of the three orthogonal lines, i.e. directly towards one of the neighbouring lithium nuclei, and when the excitations are $E \gtrsim 60\,\mathrm{eV}$. In all other directions and at lower oscillation energies the central "dent" is important because it holds the deuteron in its place.

Therefore, a good approximation for the potential $V_d(x)$ is a square well. Moreover, we can replace it with an infinitely deep square well, because the excitations that we are going to consider ($E \lesssim 100\,\mathrm{keV}$) are very small as compared to $V_{\max} \sim 1\,\mathrm{MeV}$. The advantage of

using the infinite square well is that we know both the spectrum and wave functions for such a potential analytically:

$$E_n = \frac{\pi^2 \hbar^2 n^2}{8\mu_d R_0^2} \ , \qquad \psi_n(x) = \frac{1}{\sqrt{R_0}} \sin \frac{\pi n (R_0 + x)}{2R_0} \ , \qquad n = 1, 2, 3, \dots \ , \tag{9}$$

where μ_d is the deuteron mass. Apparently, everything that was said about the potential well for the deuteron, is valid for the lithium nucleus as well. The only parameter that is different in such a case, is the mass of the nucleus. The ground-state energies for both nuclei in the corresponding potential wells are very low, namely, $E_1(d) \approx 0.6\,\mathrm{meV}$ and $E_1(\mathrm{Li}) \approx 0.2\,\mathrm{meV}$. The excitation levels are very dense. On the interval $E \in [0, 100]\,\mathrm{keV}$ there are 12,746 and 22,030 levels for the deuteron and $^6\mathrm{Li}$, respectively (see Fig. 7).

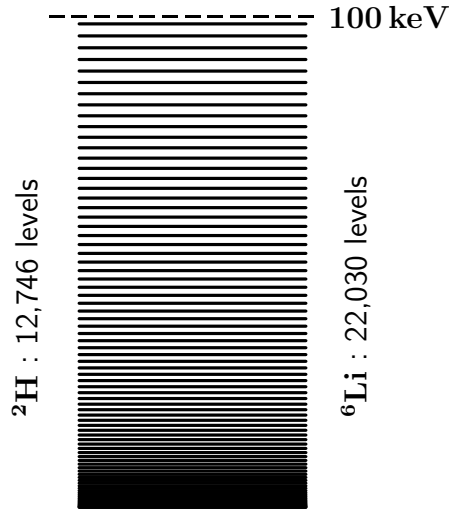

Figure 7: On the interval $E \in [0, 100]\,\mathrm{keV}$, there are 12,746 levels for the deuteron and 22,030 levels for $^6\mathrm{Li}$ in their potential wells.

3.3 Crystal under X-rays

As we have seen, in the lithium deuteride crystal the deuteron is effectively lifted up against the Coulomb barrier to the energy of $\sim 42\,\mathrm{eV}$. This gives for the exponential (Gamow) factor in Eq. (3) a negligible value,

$$E = 42\,\mathrm{eV} \quad \longrightarrow \quad \exp(-2\pi\eta) \sim 10^{-345} \ .$$

Such a small value means that the spontaneous fusion in the crystal (although is possible in principle) is far beyond our capacity to detect it.

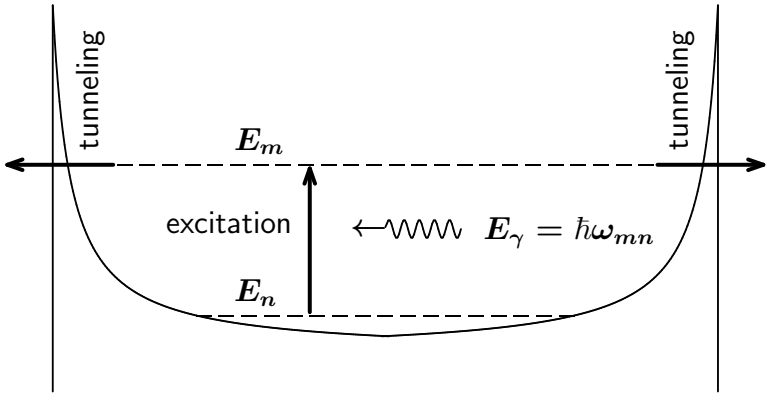

Figure 8: The deuteron gets the energy from the X-rays and tunnels through the Coulomb barrier towards the ^{6}Li nucleus.

The main idea of the experiment that we describe in the present paper, is to irradiate the crystal with X-rays, which may excite the oscillations of the nuclei (near their equilibrium positions) to such a level where they could tunnel through the Coulomb barrier as is shematically shown in Fig. 8. Apparently, the higher the excitation energy is, the greater the penetration probability would be.

3.3.1 Stimulated transitions

Under the influence of an electromagnetic wave, the stimulated excitation (or de-exitation) rate p_{mn}, i.e. the probability of transition from a state $|\psi_n\rangle$ to another state $|\psi_m\rangle$ per second, can be found as (taking into account only the dominant dipole transitions) [16]:

$$p_{mn} = \frac{4\pi^2 Z^2 e^2}{\hbar^2} \left|\langle\psi_m|x|\psi_n\rangle\right|^2 \cos^2\theta \rho(\omega_{mn}) \ , \tag{10}$$

where $Z = 1$ (for deuteron) or $Z = 3$ (for lithium), θ is the angle between the x-axis and the polarization of the photon, $\omega_{mn} = |E_m - E_n|/\hbar$, and $\rho(\omega)$ is the volume density of electromagnetic energy per unit frequency interval. Since we use lithium deuteride in the form of powder, the angle θ is random. Relative to the photon polarization, the x-axis can have any orientation uniformly distributed within full 4π solid angle. The averaging of $\cos^2\theta$ over this solid angle gives a factor of $1/3$.

The dipole matrix element in Eq. (10) can be found using the wave functions (9),

$$\langle\psi_m|x|\psi_n\rangle = \frac{2R_0}{\pi^2}\left[(-1)^{m+n}-1\right]\left[\frac{1}{(m-n)^2}-\frac{1}{(m+n)^2}\right] . \tag{11}$$

As it should be, this matrix element is non-zero only if m and n have different parities. In such a case $(-1)^{m+n}-1=-2$ and

$$\langle\psi_m|x|\psi_n\rangle = -\frac{16R_0mn}{\pi^2(m^2-n^2)^2} . \tag{12}$$

Using the first of Eqs. (9), we can replace m and n with the corresponding energies E_m and E_n,

$$\langle\psi_m|x|\psi_n\rangle = -\frac{2\hbar^2}{\mu_d R_0}\cdot\frac{\sqrt{E_mE_n}}{(E_m-E_n)^2} , \tag{13}$$

which gives the following stimulated transition rate (averaged over the photon polarizations):

$$p_{mn} = \frac{16\pi^2Z^2e^2\hbar^2}{3\mu_d^2R_0^2}\cdot\frac{E_mE_n}{(E_m-E_n)^4}\rho(\omega_{mn}) . \tag{14}$$

As is seen, the rate of high-energy excitations ($E_m \gg E_n$) diminishes as $\sim E_m^{-3}$.

3.3.2 Population of energy levels

The statistical ensemble of deuterons in the crystal is in the thermodynamical equilibrium, and thus the population P_n of each level (i.e. the probability that a particular deuteron occupies the level n) can be found using the Boltzmann distribution,

$$P_n = \frac{\exp\left(-E_n/k_BT\right)}{\sum_{j=1}^{\infty}\exp\left(-E_j/k_BT\right)} . \tag{15}$$

At the room temperature, $T=300\,^\circ\mathrm{K}$, this distribution gives the following average energy for the oscillations of the deuteron in the square well potential:

$$\langle E\rangle_d = \sum_{n=1}^{\infty}E_nP_n \approx 14.2\,\mathrm{meV} . \tag{16}$$

The corresponding energy for the ^{6}Li-nucleus is almost the same, $\langle E\rangle_{\mathrm{Li}}\approx 13.6\,\mathrm{meV}$. These small values are obtained because only a couple of dozens of the lowest levels are populated

with appreciable probabilities.

When the crystal is exposed to X-rays, the statistical ensemble of deuterons (or similarly $^6\mathrm{Li}$ nuclei) is not in the thermodynamical equilibrium anymore. Its distribution over the energy levels is changing. The deuterons jump up and down due to absorption and emission of photons.

If the flux of external photons is steady, a new dynamical equilibrium is formed with constant population $P_m(t) = \mathrm{const}$ for each level $m = 1, 2, 3, \ldots$. The time-evolution of the populations can be described by the so called master equation (see, for example, Ref. [17]),

$$\frac{dP_m}{dt} = \sum_{n \neq m} p_{mn} P_n - \sum_{n \neq m} p_{nm} P_m + \sum_{n>m} p^{\mathrm{sp}}_{mn} P_n - \sum_{n<m} p^{\mathrm{sp}}_{nm} P_m \ , \tag{17}$$

where p_{mn} is the rate of $(m \leftarrow n)$-transition stimulated by the external radiation, and p^{sp}_{mn} is the rate of spontaneous transition from a higher level n to a lower level m. The stimulated transition rate is given by Eq. (14), and the spontaneous rate (in the same dipole approximation) can be found as [16]

$$p^{\mathrm{sp}}_{mn} = \frac{4\omega^3_{mn} Z^2 e^2}{3c^3\hbar} \left|\langle \psi_m | x | \psi_n \rangle\right|^2 \ , \tag{18}$$

involving the same matrix (13). As we said before, the elements of this matrix are non-zero only if m and n have different parities, i.e. $(-1)^{m+n} = -1$.

Using Boltzmann distribution (15) as the initial conditions at $t = 0$, we can, in principle, numerically solve the system of differential equations (17) up to such time t when all the populations reach constant values. In practice, however, this is difficult to do. The reason is that the system (17) consists of too many equations (see Fig. 7) and therefore becomes numerically unstable.

If we manage to solve the differential equations (17), we obtain much more information than we actually need. Indeed, such a solution would give us the full history of how the initial Boltzmann distribution evolves with time. But we only need the final stationary distribution, when all $P_n(t)$ reach their constant values and their derivatives on the left hand sides of these equations become zero. This gives a homogeneous system of linear equations,

$$\sum_n A_{mn} P_n = 0 \ , \tag{19}$$

with the normalisation condition

$$\sum_n P_n = 1 \ , \tag{20}$$

where the matrix A_{mn} is composed of the transition rates p_{mn} and $p^{\rm sp}_{mn}$ as is given in Eq. (17).

It is easy to proof (using the method of mathematical induction) that the symmetry of the transition rates with respect to permutations of their subscripts implies that for each column of matrix A, the sum of its elements is zero. These means that the lines of this matrix are linearly dependent and thus $\det A = 0$. In other words, the linear system (19) always has a unique non-trivial solution, no matter what the initial distribution is.

A homogeneous linear system with the additional condition (20) and the symmetry properties described above, can be transformed to an equivalent non-homogeneous system, which can be numerically solved using the Gauss-Seidel iterative procedure. An algorithm for such a solution can be found in Ref. [18].

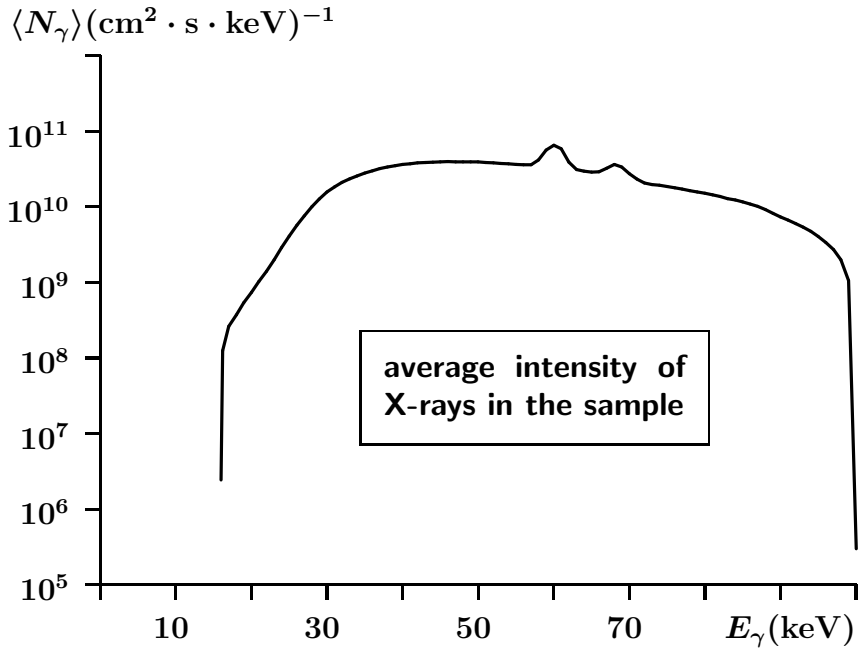

Figure 9: Number of photons in the unit energy interval, bombarding $1\,\mathrm{cm}^2$ of the target cross section during one second. The number is averaged over the thickness of the sample.

In our experiment, we irradiated the sample with the X-rays whose spectrum covered the

energy interval of $[15, 100]\,\mathrm{keV}$. The sample consisted of many layers of lithium deuteride alternated with polymer detectors (for details, see Sec. 4.1). The total depth of the sample along the direction of the radiation was $13\,\mathrm{cm}$. The radiation intensity attenuated in the sample due to absorption and the divergence of the rays. In our calculations, we used the intensity averaged over the depth of the sample. The averaged spectrum of X-rays is shown in Fig. 9. It is given in terms of the number N_γ of photons in the unit energy interval falling on the area of $1\,\mathrm{cm}^2$ per second.

Using this spectrum, $N_\gamma(E)$, we calculated the corresponding volume density $\rho(\omega)$ of electromagnetic energy per unit frequency interval as follows. In one cubic centimeter, there are those photons that fall on $1\,\mathrm{cm}^2$ of its side during the time $1\,\mathrm{cm}/c$ needed for the first bunch of photons to reach the opposite side of the 1 cm cube. The total electromagnetic energy in the cube is the number of photons multiplied by $\hbar\omega$. Dividing this by ω, we obtain the energy density per unit frequency, $\rho(\omega) = N_\gamma \hbar/c$.

This density is needed in finding the stimulated transition rates (14). With these rates and the rates (18) of the spontaneous transitions, we solved the linear system (19) and thus found the stationary probability distribution for occupying various energy levels in the potential square-well. This was done for both the deuteron and $^6\mathrm{Li}$ nuclei (the only difference is the mass). The resulting distributions are shown in Fig. 10.

3.4 Fusion induced by X-rays in the crystal

When the crystal is exposed to the X-rays, the nuclei oscillating within the square-well potentials, acquire some kinetic energy. As a result, the probability for them to penetrate through the Coulomb barrier increases. The corresponding fusion rate for a deuteron (and similarly for lithium) is given by Eq. (5).

In that equation, the energy E does not have a definite value, but can be any E_n of the square-well spectrum for the deuteron (or lithium, which is different), with the probability distributions $P_d(E)$ and $P_{\mathrm{Li}}(E)$ shown in Fig. 10. This is similar to the reactions in stellar plasma [19], where velocities of the colliding nuclei are distributed according to Maxwell's probability density. Therefore the observable fusion rate is the following average

$$\langle W_i \rangle = \sum_n W_i(E_n^{(i)}) P_i(E_n^{(i)}) \;, \tag{21}$$

where i stands for either d or Li.

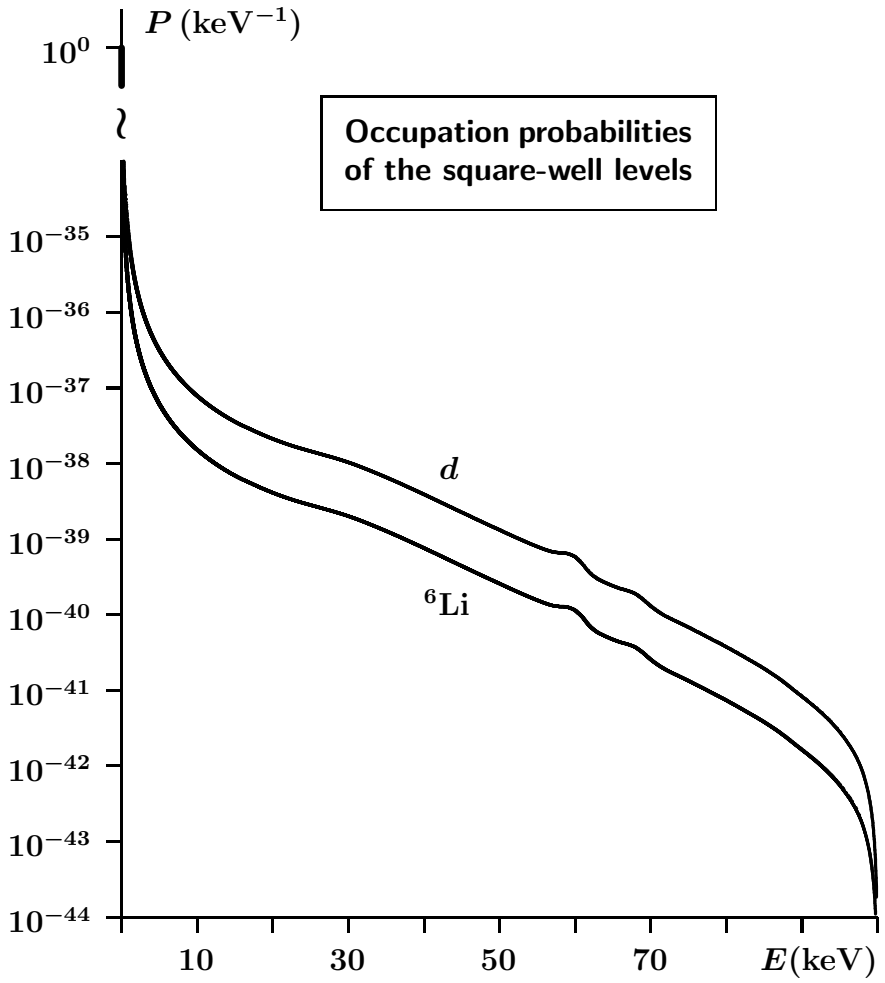

Figure 10: Probabilities (per unit energy interval) of populating the levels in the square-well potential for the deuteron and $^{6}\mathrm{Li}$ nuclei, when the crystal is exposed to the X-rays with the spectrum shown in Fig. 9.

Each deuteron has six neighbouring lithium nuclei and similarly each lithium nucleus has six hydrogen isotopes surrounding it. However, the crystal is not pure $\mathrm{D}^{6}\mathrm{Li}$ compound. In some nodes of the lattice it can be a proton (instead of d) or $^{7}\mathrm{Li}$ (instead of $^{6}\mathrm{Li}$). In our experiment, it was used a sample containing $M = 0.61\,\mathrm{g}$ of lithium hydride powder with natural isotope composition of lithium (mass fractions of $^{6}\mathrm{Li}$ and $^{7}\mathrm{Li}$ being $f_6 = 0.0759$ and $f_7 = 0.9241$, respectively) and enriched with the hydrogen isotope $^{2}\mathrm{H}$ ($f_1 = 0.02$ and $f_2 = 0.98$).

Therefore, if you find a hydrogen atom in the crystal, it is a deuterium with the probability of f_2. And a lithium atom has in its centre the $^6\mathrm{Li}$ isotope with the probability of f_6. Therefore, a deuteron can find around itself a $^6\mathrm{Li}$ nucleus with the probability of $6f_6$, and for a $^6\mathrm{Li}$ isotope the probability to find a deuteron nearby is $6f_2$.

Since there are two possibilities for the same fusion event to happen: either the deuteron or the lithium gets through the barrier, the total ("bulk") fusion rate for the whole crystal can be found as a sum of the corresponding contributions:

$$R = 6f_6 N_d \langle W_d \rangle + 6f_2 N_{\mathrm{Li}} \langle W_{\mathrm{Li}} \rangle \ . \tag{22}$$

where N_d and N_{Li} are the numbers of available deuterons and $^6\mathrm{Li}$ nuclei.

The effective molar mass m of our crystal-powder is

$$m = f_1 1\,\mathrm{g} + f_2 2\,\mathrm{g} + f_6 6\,\mathrm{g} + f_7 7\,\mathrm{g} \ . \tag{23}$$

The number of hydrogen and lithium atoms (any isotopes) is the same, namely, $(M/m)N_A$, where N_A is the Avogadro number. This gives

$$N_d = \frac{M}{m} N_A f_2 \ , \qquad N_{\mathrm{Li}} = \frac{M}{m} N_A f_6 \ , \tag{24}$$

and therefore

$$R = 6\frac{M}{m} N_A f_2 f_6 \Big(\langle W_d \rangle + \langle W_{\mathrm{Li}} \rangle \Big) \ . \tag{25}$$

Numerical calculations with the X-ray spectrum shown in Fig. 9, give the following results for the single-nucleus rates:

$$\langle W_d \rangle \approx 2.4 \times 10^{-26}\,\mathrm{s}^{-1} \ , \qquad \langle W_{\mathrm{Li}} \rangle \approx 4.6 \times 10^{-27}\,\mathrm{s}^{-1} \ . \tag{26}$$

The corresponding "bulk" rate for the whole sample is

$$R \approx 5.2 \times 10^{-4}\,\mathrm{s}^{-1} \ . \tag{27}$$

For the total exposure time in our experiment, $t = 111.466$ hours, we therefore should have expected to register $N \sim 207$ fusion events.

4 Experiment

As it follows from the theoretical estimate (see previous Section), the fusion events we are looking for, are rare (roughly, one event every half an hour). This fact determines the sample design and the choice of the way of registering the events. The low rate of the reaction implies that we need to expose the sample to the X-rays for a relatively long time (at least a hundred hours) to get a statistically meaningful result. The detector should be able to efficiently distinguish the fusion events from all possible background signals and to accumulate the information during whole exposure period.

Based on this, we used the polymer track detectors CR-39 in direct contact with the active material (lithium hydride). Each fusion event results in a pair of α-particles moving in the opposite directions with the same energy of $11.1863\,\mathrm{MeV}$. These particles leave tracks in the polymer material, which can be identified after the experiment is completed. Since only few hundred events are expected, the probability that different tracks overlap each other is practically zero. The background tracks left by other charged particles, can be easily excluded using specific properties of the tracks belonging to the α-particles from the fusion events (see Sec. 4.4).

4.1 Sample preparation

Lithium hydride (LiH) is a solid crystalline compound, usually available in the form of chunks or powder. It is extremely hygroscopic, absorbing water from the air, via the chemical reaction

$$\mathrm{LiH} + \mathrm{H_2O} \longrightarrow \mathrm{LiOH} + \mathrm{H_2}\ .$$

For our experiment, this is a destructive process and therefore we avoided the contacts of LiH with atmospheric air by all available means. All the manipulations with the crystals were done in an anaerobic chamber (glove-box) filled with dry $\mathrm{CO_2}$ gas. Besides that, some desiccants were present in the chamber.

The crystalline chunks were ground into powder form. This powder was placed between square plates ($1\,\mathrm{cm}^2$ each) of the plastic detectors (CR-39), as is schematically shown in Fig. 11. We put in parallel several units like the one shown in this Figure, and the whole assembly was enclosed in a hermetic PVC container. The total number of the detector plates was 85.

The lithium hydride we used, was not pure $\mathrm{D}^6\mathrm{Li}$-compound. The isotope composition of

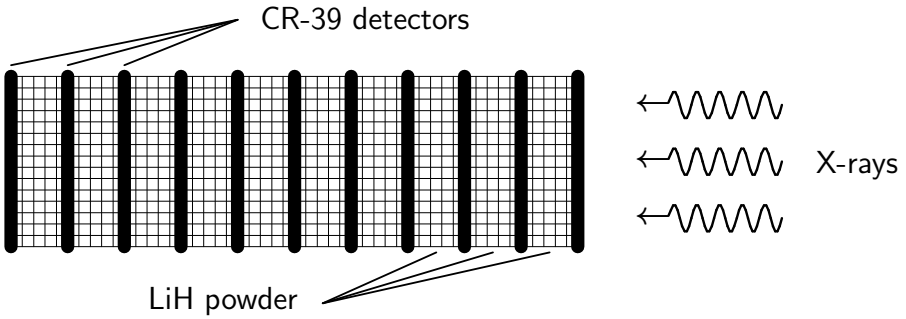

Figure 11: Schematic picture of a sample unit composed of alternating layers of lithium-deuteride powder and the plastic detectors (CR-39). Whole assembly includes several units like this, placed parallel to each other inside a hermetic PVC container. The distance between the detector plates is 1 cm. The total number of the detectors in whole assembly is 85. Each detector plate is a square of the area 1cm$\times$1cm with 1 mm thickness. The X-rays are directed perpendicular to the plates.

lithium atoms was practically natural, namely, 92.41% of $^7\mathrm{Li}$ and 7.59% of $^6\mathrm{Li}$. As far as the hydrogen atoms are concerned, the substance was enriched with deuterium up to 98%.

4.2 X-ray source and spectrum

To generate the X-rays, we used a XYLON Y.TU 225-D02 tube. The tube was operated with a potential difference of 100 kV and the current of 30 mA. In order to find out what was the spectrum of the rays, we used available data for the spectrum of this source, measured at the same voltage, but with a much lower current, namely, $0.1\,\mu\mathrm{A}$, and at a different distance. We simply scaled these data to actual current and distance, used in our experiment.

The length of our sample was 13.2 cm. Passing through the sample, the X-rays attenuate both because of interaction with the material and because of spreading (the rays are not collinear). As a result the intensity of the radiation is not uniform through the sample. In our theoretical estimate, we used average intensity of the X-rays in the sample. The corresponding spectrum (obtained by scaling the original data and averaging them) is shown in Fig. 9.

4.3 Background

We identify the fusion events by registering the α-particles that emerge from the decay of the resulting $^8\mathrm{Be}^*(22.2\,\mathrm{MeV})$ resonance. However, there are other (background) sources

of α-particles that might be distorting our counting. Among them the most common is radon (and its decay products) that is present practically everywhere. In addition to that, our measurements were done at the premises of NECSA (Nuclear Energy Corporation South Africa) near Pretoria, where a nuclear reactor was operating. Although an appropriate radiation shielding was used, we cannot exclude that some thermal neutrons from the reactor could reach our sample and generate α-particles in collisions with $^6\mathrm{Li}$ via the reaction

$$n + {}^6\mathrm{Li} \;\longrightarrow\; \alpha + t + 4.78\,\mathrm{MeV}\ . \tag{28}$$

Our detectors were kept isolated from the atmospheric air all the time. And since α-particles cannot penetrate through a plastic container, we can safely ignore the possibility of counting false events due to radon and its progeny. The only source of possible false events is the reaction (28). However, the α-particles from the fusion events have a much higher energy (11.1 MeV) than those from this reaction. This fact provides us with a reliable way of distinguishing the fusion and false events. When analysing the detectors, we only counted the tracks left by particles with the energy higher than 6 MeV (for the details see Sec. 4.4).

4.4 Detector processing

The fusion events were registered by identifying the appropriate tracks left by α-particles in the solid state nuclear track detectors CR-39. Original tracks are very narrow channels where the structure of the plastic material is damaged by the particle. These channels become much wider and visible under a microscope magnification, after etching. For etching, we used a 6.25 mol/ℓ solution of NaOH at 70 °C.

This solution removes the plastic material not only from the channels, but from all the surfaces. However the rate of etching at the damages is higher. There are certain empirical formulae that enable one to calculate the etching rates at various conditions (see Ref. [20] and the references therein). It is therefore possible to numerically model the shapes of the tracks for different etching times. For such a modelling, we used the standard code TRACK_TEST developed by the authors of Ref. [21].

Depending on its kinetic energy, the α-particle penetrates into the plastic material and damages it to a certain depth (typically a dozen of microns). When etched, such a track forms a pit in the shape of a sharp cone, as is shown in Fig. 12(a). The longer we etch it, the deeper and wider this cone becomes. This goes on until the depth of the pit becomes equal to the penetration length. After that the pit only becomes wider and retains practically the same depth. As a result, the bottom of the pit transforms from a sharp cone to a smooth

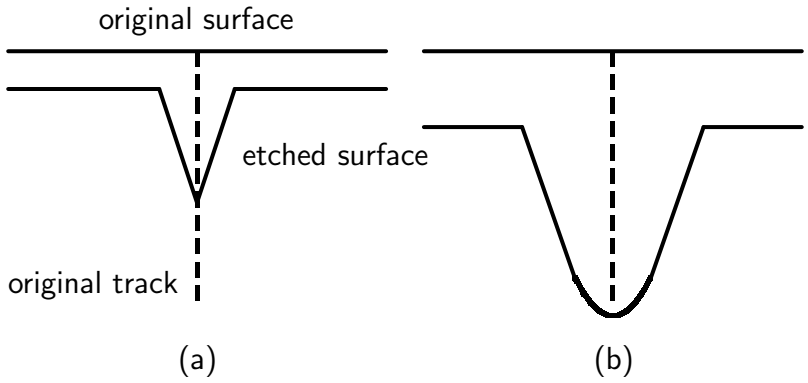

Figure 12: Schematic representation of the etching process for two different durations: (a) Etching time is not sufficient to reach the bottom of the original track; (b) Rounding of the bottom of the pit after the track end has been reached.

spherically concave surface, as is schematically shown in Fig. 12(b).

The sharp cone and concave shapes have different optical properties. A smooth concave surface reflects the light and even focus it to a small dot, which is not possible for a sharp cone. Therefore just looking into the etched tracks, we can distinguish "finished" (track end has been reached) and "unfinished" tracks. Using the TRACK_TEST software, we can calculate the length of the track for any given energy E_α of the α-particle as well as calculate the depth of the pit for a given etching time t. Therefore we can choose t such that all the tracks for E_α higher than certain threshold $E_{\min}$, form sharp cone pits, while for $E_\alpha < E_{\min}$ the pits reflect the light.

Since we need to exclude the tracks resulted from the reaction (28), where the maximal energy is 4.78 MeV, we could choose the threshold energy to be 5 MeV. However, to be absolutely sure, we used $E_{\min} = 6\,\mathrm{MeV}$. This corresponds to etching time $t = 8$ hours. After the etching, we looked for completely dark pits (sharp cones) with certain diameter of the opening. These tracks could not be done by anything else but the α-particles from the fusion reaction.

4.5 Efficiency of the detecting

It should be noted that we cannot register all the fusion events that occur in the sample. First of all, the α-particles from the reactions that take place far away from a detector plate, cannot reach the detector because the distance they can go through in any solid media is very short.

Moreover, even if they reach a detector surface from afar, they loose a significant part of the kinetic energy and thus cannot be registered if the remaining energy is less than $E_{\min} = 6\,\mathrm{MeV}$.

Our calculations show that in the lithium-hydride the original energy of 11.1 MeV of the α-particle is reduced to the minimally acceptable energy of 6 MeV on the distance of $x_{\max} = 0.095\,\mathrm{mm}$. This means that, when we count the events, we can only register the events happening within a thin layer of the lithium-hydride of 0.095 mm thickness, which is in contact with the detector. Since in total we have 85 detectors and for each of them the surface area in contact with LiH is $0.95 \times 0.95\,\mathrm{cm}^2$ (most of them have LiH on both sides), the total volume of LiH, from which we register the α-particles, is $0.77\,\mathrm{cm}^3$ and the corresponding mass is 0.61 g. This effective mass of the active material was used in our theoretical estimate of the fusion rate.

This is not the end of the story. The efficiency of the detection is reduced further by the fact that the α-particles are emitted isotropically in all directions. For example, if the fusion event happens at the maximal acceptable distance from the detector and the α-particle moves at a non-zero angle relative to the normal to the detector surface, the actual distance it has to pass in LiH is greater than the $x_{\max}$ and thus it looses too much energy. Similar losses take place at any distance within the thin layer, when the angle is too large. Moreover, the tracks with the angle to the normal greater that 45° cannot be identified using our simple method.

Estimating all possible losses, we conclude that we can only register of about 40% of the events happening in 0.61 g of the material. This means that from the number of detected events we can only derive a lower bound for the reaction rate. This is sufficient for a first and simple experiment. Actually, the main goal of our experiment was to establish if the fusion in the crystal could be induced by X-rays or not.

5 Results and discussion

The sample composed of alternating layers of lithium-hydride and the plastic detector-plates (as is described in Sec. 4.1), was exposed to the X-ray radiation for the duration of 111.466 hours. Then, after the etching of the detectors, we identified (in total on all 85 plates) 88 tracks that belonged to the α-particles from the fusion reaction (2). Since we could not register all the fusion events (some of them were missing as is explained in Sec. 4.5), actual number N of the events (happened in 0.61 g of LiH) is greater, $N > 88$. Taking into account that the substance we used was not pure lithium-deuteride (see Sec. 3.4 for explanations), we conclude that under the used electromagnetic radiation (the spectrum is given in Fig. 9) the

fusion rate for a single $d - {}^6\mathrm{Li}$ pair is

$$R_{d^6\mathrm{Li}} > 1.19 \times 10^{-26}\,\mathrm{s}^{-1}\ .$$

This result is of the same order of magnitude as was predicted by our theoretical estimate (26). The total number of events $N = 207$, theoretically expected for our experimental conditions and duration, is in accordance with the actual observation, $N > 88$.

Apparently, the fusion rate turned out to be too low for any possible applications of this process in the energy production. However, the electromagnetically induced nuclear reactions in crystals can be used in a different way. In principle, this offers a new way of measuring the cross sections (or the astrophysical S-factors) of such reactions (not only fusion) at extremely low energies, which are not accessible in the direct collision experiments.

Of course, such an approach would require a more rigorous theoretical description of all the processes involved. In particular, the electron screening has to be taken into account in a proper way. This could be done by appropriately modifying the barrier penetration factor and using an accurate model (instead of the square well) for the potential schematically shown in Fig. 6. There is no doubt that taking into account the electron clouds is not an easy task. Indeed, the configuration of their space charge is dynamically changing when the nuclei move. It is therefore needed some theoretical effort before the nuclear reactions in crystals could be used for measuring the corresponding cross sections at low energies.

At present, the only alternative to the direct collision experiments at low energies is the so called "Trojan Horse" method, where the projectile is carried to the close proximity of the target as a cluster inside another nucleus (the "horse"). This "horse" may have the kinetic energy well above the Coulomb barrier and thus neither its penetrability nor the screening effects play any role. When near the target, the projectile is detached from the "horse" and interacts with the target at a low energy while practically all the original kinetic energy is taken away by the "empty horse" (see [22], and the references therein).

Although in the "Trojan Horse" method the complicated screening effects are avoided, it still relies on an involved theoretical analysis. Therefore, an additional experimental method for determining the S-factors would be of help. The "Trojan Horse" and the crystal methods would complement each other.

Experimentally, the main advantage of using crystals is the fact that here the effective flux of the nuclei is extremely dense. Indeed, roughly the Avogadro number of projectiles collide

with the Avogadro number of target nuclei. With such a density (as we have seen in our experiment) even the reactions with very low probabilities can be observed. In order to narrow the interval of the collision energies, a synchrotron radiation can be used instead of the X-rays.

References

[1] R. Balian, J.-P. Blaizot, P. Bonche, *"Cold fusion in a dense electron gas"*, J.Phys. France, **50**, 2307-2311 (1989)

[2] A.C. Sips, G. Giruzzi, S. Ide, C. Kessel, T.C. Luce, J.A. Snipes, J.K. Stober, *"Progress in preparing scenarios for operation of the International Thermonuclear Experimental Reactor"*, Physics of Plasmas, 2015, **22(2)**, pp. 1-24 (2015).

[3] H. S. Picker, *"On the fusion of hydrogen isotopes in ordinary molecules"*, Nucleonica, **25**, 1491-1494 (1980)

[4] J. D. Jackson, *"Catalysis of nuclear reactions between hydrogen isotopes by μ^- mesons"*, Phys. Rev., **106**, 330-339 (1957)

[5] H.E. Rafelski, D. Harley, G.R. Shin, J. Rafelski, *"Cold fusion: muon-catalysed fusion"*, J.Phys. B: At.Mol.Opt.Phys., **24**, pp. 1469-1516 (1991).

[6] D.V. Balin et al., *"High Precision Study of Muon Catalyzed Fusion in D2 and HD Gases"*, Physics of Particles and Nuclei (JINR, Dubna), v. 42(2), pp. 361-414 (2011).

[7] S. E. Jones, *"Muon-catalysed fusion revisited"*, Nature, **321**, pp. 127-133 (1986).

[8] V. B. Belyaev, M. B. Miller, Yu. G. Sobolev, A. V. Sermyagin, I. V. Kuznetzov, and E. Bialkovski, *"Molecular-Nuclear Transition ^{6}LiD $\rightarrow$ ^{6}Be*: Search with a Paired $\Delta E - E$ Telescope"*, Few-Body Systems, **38**, pp. 103-107 (2006).

[9] D. R. Tilley, J. H. Kelley, J. L. Godwin, D. C. Millener, J. E. Purcell, C. G. Sheu, H. R. Weller, *"Energy levels of light nuclei $A = 8, 9, 10$"*, Nucl. Phys., **A745**, pp. 155-362 (2004).

[10] J. Grineviciute, L. Lamia, A.M. Mukhamedzhanov, C. Spitaleri, M. La Cognata, *"Low-energy R-matrix fits for the ^{6}Li$(d, \alpha)^4$He S factor"*, Phys. Rev., **C91**, 014601 (2015).

[11] L. D. Landau, E. M. Lifshitz, *"Quantum Mechanics"*, Pergamon Press, (1965).

[12] D. Laplaze, *"Lattice dynamics of lithium hydride and lithium deuteride: effect of long-range tree-body forces"*, J.Phys.C: Solid State Phys., **C10**, pp. 3499-3520 (1977).

[13] Table XLI of: P. J. Mohr, B. N. Taylor, D. B. Newell, *"CODATA recommended values of the fundamental physical constants: 2010"*, Rev.Mod.Phys., **84(4)**, pp. 1527-1605 (2012).

[14] E. G. Nadjakov, K. P. Marinova, Yu. P. Gangrsky, *"Systematics of nuclear charge radii"*, Atomic Data and Nuclear Data Tables, **56**, pp. 133-157 (1994).

[15] A. Bohr, B. R. Mottelson, *"Nuclear Structure"*, Volume I, p.173, W. A. Benjamin, inc., New York, Amsterdam (1969).

[16] D. I. Blokhintsev, *"Quantum Mechanics"*, D. Reidel Publishing company, Dordrecht, Holland (1964).

[17] N. G. Van Kampen, *"Stochastic Processes in Physics and Chemistry"*, Third Edition, NORTH-HOLLAND (2007).

[18] http://www.mathpages.com/home/kmath175/kmath175.htm

[19] C. E. Rolfs, W. S. Rodney, *"Cauldrons in the Cosmos"*, The University of Chicago Press, Chicago, (1988).

[20] A. A. Azooz, S. H. Al-Niaemi, M. A. Al-Jubbori, *"A parameterization of nuclear track profiles in CR-39 detector"*, Computer Physics Communications, vol. 183, pp. 2470-2479 (2012).

[21] D. Nikezic, K. N. Yu, *"Computer program TRACK_TEST for calculating parameters and plotting profiles for etch pits in nuclear track materials"*, Computer Physics Communications, vol. 174, pp. 160-165 (2006).

[22] C. Spitaleri et al., *"Measurement of the 10 keV resonance in the* $^{10}\mathrm{B}(p,\alpha_0)^7\mathrm{Be}$ *reaction via the Trojan Horse method"*, Phys. Rev., **C90**, 035801 (2014).